Growth Modulation of Super-tetragonal PbTiO3 Thin Films with Self-Assembled Nanocolumn Structures

Zeyu Zhang,[1] Yanzhu Dai,[2] Zhipeng Li,[1,] Lu Lu,[2] Xin Zhang,[1] Kunwu Fu,[3] Xiaoguang Xu,[1] Wenhuai Tian,[1] Chun-Lin Jia,[2,4,] Yong Jiang[1,*]*

Z. Zhang, Prof Z. Li, X. Zhang, Prof X. Xu, Prof W. Tian, Prof Y. Jiang
School of Materials Science and Engineering, Beijing Advanced Innovation Center for Materials Genome Engineering, University of Science and Technology Beijing, Beijing, 100083, China
Email: zplmse@ustb.edu.cn, yjiang@ustb.edu.cn
Y. Dai, L. Lu, Prof C.-L. Jia
The School of Microelectronics and State Key Laboratory for Mechanical Behaviour of Materials, Xi'an Jiaotong University, Xi'an, 710049, China
Dr K. Fu
Bruker (Beijing) Scientific Technology Co., Ltd, Beijing, 100192 China
Prof C.-L. Jia
Ernst Ruska-Centre for Microscopy and Spectroscopy with Electrons (ER-C), Forschungszentrum Jülich GmbH, 52425 Jülich, Germany

Abstract

Although the epitaxial strain due to lattice mismatch between films and substrates could lead to improved properties and emergent functionalities, the limited choices of substrates and strain relaxation has hindered the further tunning of thin films ferroelectricity by conventional strain engineering via electro-elastic coupling. Here, we fabricate epitaxial thin films composed of self-assembled arrays of $Pb_xTi_yO_{x+2y}$ (lead-riched) nanocolumns embedded in a $PbTiO_3$ matrix by laser ablation of single lead titanate ceramic targets. The c-axis lattice parameter of the whole nanostructure can reach up to 4.7 Å and the out-of-plane to in-plane lattice parameter ratio of 1.2 could be achieved, based on which spontaneous polarization is also estimated according to the coupling between tetragonality and polarization for ferroelectrics. The value of tetragonality could be well tuned by the growth conditions, such as the growth temperatures. Moreover, single lead titanate film composed of multiple tetragonalities could also be reached. Our work provides a general approach to regulation of

lattice states and functionalities beyond their present levels via elastic coupling between the self-assembled nanostructures in three dimensions.

1. Introduction

The electronic materials with multifunctionalities are of fundamental interest and technological importance for applications in information techniques. [1-3] Ferroelectrics featuring electrical switchable polarization are promising candidate for the microelectronic devices such as sensors, transducers and nonvolatile memory devices. [4,5]The high performance of ferroelectric oxides with perovskite structure including the large polarization and high Curie temperature is usually related to their giant tetragonality (*c/a*) of lattices.[6-13] However, this kind of compounds are rare and require extreme synthesis conditions, e.g., applying high compressive strain by diamond anvil cells.[9,14] Recently, significant development of thin film growth techniques has enabled high quality epitaxial ferroelectric films with improved properties and emergent functionalities. The strain engineering including lattice strain which is due to the lattice mismatch between film materials and substrates, as well as the thermal strain has become a well-recognized approach for manipulation of lattice deformation and physical properties. [7,15,16]However, this approach is basically hampered due to limited commercially single crystal substrates or film-thickness driven strain relaxation.

In light of these challenges, additional growth parameters could be introduced for extending new structures and properties. Recent works demonstrated that by synergetic controlling of the laser fluence, lattice strain, and thermal strain, highly strained tetragonal phase (*c/a*~1.1) of $PbTiO_3$ films with large Poisson's ratio and polarization could be reached.[17] Moreover, by introducing another phase into ferroelectrics to form a nanocomposite material, polarization could also be strongly enhanced.[18] Lin et al. used the laser ablation of $BaTiO_3$:$SrRuO_3$ (BTO:SRO) ceramic target and fabricated SRO nanoclusters embedded in epitaxial BTO film matrix, realizing increase of polarization in BTO film.[19] Zhang et al. introduced a large interphase strain in the magnetron sputtering deposited $PbTiO_3$:PbO composites which have dispersed PbO nanoparticles in the films and found giant tetragonality of the ferroelectric films.[20] Here, we fabricated epitaxial thin films with self-assembled arrays of $PbTiO_3$ nanocolumns intergrowing with (Pb,Ti)O phase with PbO structure by laser ablation of single lead titanate target. The X-ray diffraction characterization suggests the c-axis parameter of the whole nanostructure can reach up to 4.71 Å and the lattice tetragonality up to 1.23 could be achieved (compared to 1.065 in bulk) measured by electron diffraction. The spontaneous polarization is also estimated according the coupling

between polarization and tetragonality. The value of tetragonality could be well tuned by the growth conditions, such as the growth temperatures. Moreover, single lead titanate film composed of multiple tetragonalities could also be reached. This work provides a new pathway to effectively modulate and enhance ferroelectricity by developing emergent nanostructures.

2. Results and Discussion

$PbTiO_3$ has a tetragonal perovskite structure with lattice parameters (a = 3.899 Å, c = 4.154 Å, and *c/a* = 1.065).[21] The epitaxial $PbTiO_3$ (PTO) films were grown on perovskite single crystal substrates by pulsed laser deposition (PLD). $La_{0.7}Sr_{0.3}MnO_3$ (LSMO) was used as the bottom electrode. As described below, the growth conditions, such as substrate temperature, oxygen pressure can be used to control the microstructure of thin films. Figure 1a and 1b show the X-ray diffraction results and analysis of PTO/LSMO heterostructures grown on $SrTiO_3$ (STO) (001) substrates by varying the film growth temperatures. Only c-axis diffraction peaks could be observed, showing the films were epitaxially grown. The shift of PTO diffraction peaks to lower angles demonstrates the apparent change of c-axis lattice parameters by tuning growth temperatures. It is found that as the growth temperature gradually increases (540→600→700 ℃), the c-axis lattice parameter gradually increases and then sharply decreases (4.65→ 4.71→4.12 Å) (film thickness were maintained to be 18 nm, oxygen pressures are 2 Pa). For example, the c-axis epitaxial PTO film deposited at growth temperature of 600 ℃, the c lattice can be extended by 13.3% compared with its bulk counterpart. Here, the PTO phase with c-axis lattice parameter larger than 4.4 Å is called super tetragonal phase (ST), while the one with c lattice value near 4.15 Å is called normal tetragonal phase (NT). Figures 1c and 1d show the thin film thickness effect on the change of c-axis lattice parameter when films were grown on 600 ºC and 700 ºC, corresponding to the ST and NT phase, respectively. Figure 1e presents the quantitative analysis. It shows the c lattice parameter of ST phase decreases from 4.71 Å to 4.537 Å when film thickness increases from 18 nm to 54 nm (substrate temperatures during growth were 600 ºC and oxygen pressures were 2 Pa), while the c lattice value of NT phase is nearly 4.15 Å. It is known that as the thickness increases, the compressive strain from the substrate on the PTO would gradually relax, resulting in the increase of *a*-axis lattice value and decrease of c-axis lattice value. It indicates that the growth of the ST phase in this system is simultaneously affected by the epitaxial strain from substrate. The results are on the contrary of Zhang's work in which the c-axis lattice value of super-tetragonal PTO increases with the increase of film thickness.

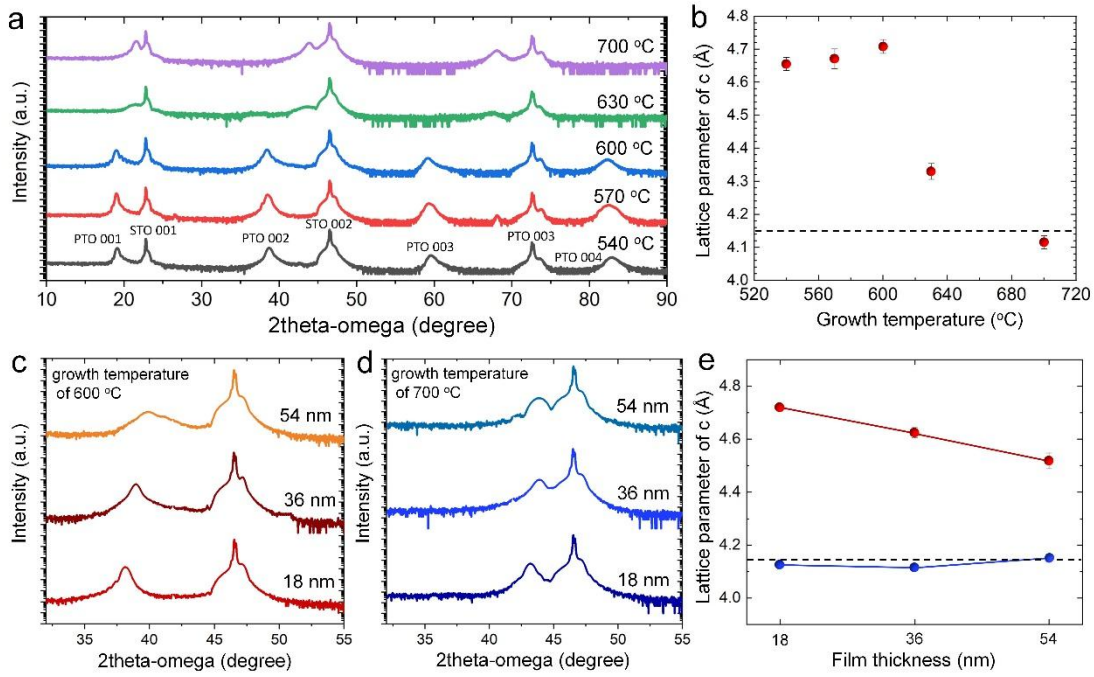

Figure 1. a) Growth temperature-dependent XRD of PTO(20nm)/LSMO/STO (001) systems. b) The c-axis lattice parameter as a function of growth temperature. c) and d) The thickness-dependent XRD of PTO/LSMO/STO (001), with growth temperature of 600 °C and 700 °C, respectively. e) The c-axis lattice parameter as a function of thickness at different growth temperature (red: 600 °C, blue: 700 °C). The black dashed lines indicate the c-axis lattice parameter of bulk PTO.

For the ST sample grown at 600°C, we further explore the effect of oxygen pressure on the lattice parameters, as shown in Figure 2a and b. It is noted that the formation of ST phase is also sensitive to oxygen pressure (Figure 2a). The c-axis lattice parameter decreases with increase of oxygen pressure. Generally, the single ST phase can be maintained with an oxygen pressure of less than 2 Pa. As the pressure increases to 10 Pa, an additional NT phase gradually appears, resulting the coexistence of ST and NT phase (c_{ST}=4.625 Å, c_{NT}=4.188 Å) in one sample. Moreover, different substrates including (La,Sr)(Al,Ta)O_3 (LAST) and $LaAlO_3$ (LAO) were used to grow PTO films to study the strain effect (with substrate temperature of 600 °C and film thickness of 18 nm). Since the in-plane lattice parameters of LSAT and LAO are smaller than that of STO, it would bring greater compressive stress to the PTO film. The results are shown in Figure 2c and d. It is demonstrated that the larger compressive stress enables the PTO of NT phase and HT phase to coexist in the PTO film grown at 600°C. The c lattice parameter values of their corresponding ST phases (4.77 Å) are slightly larger than the pure ST phase grown on STO, originating from larger compressive strain. More interestingly,

when the growth temperature increases to 620°C, the PTO film grown on the LAO, a diffraction peak corresponding to intermediate phase (c=4.11 Å) appeared in the XRD pattern, suggesting coexistence of three phases in one sample.

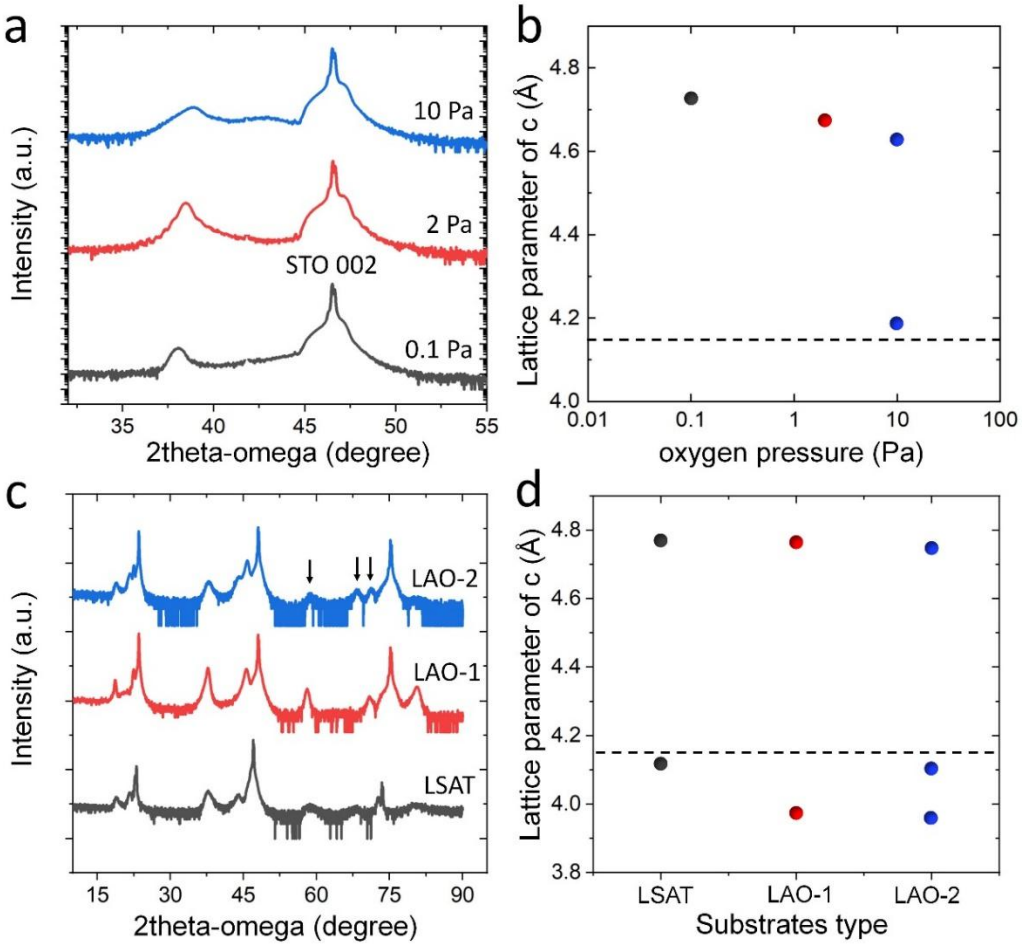

Figure 2. a) Oxygen pressure-dependent XRD of PTO/LSMO/STO (001). b) The c-axis lattice parameters as a function of oxygen pressure. c) XRD of PTO/LSMO heterostructures on different substrates. The black arrows indicate the (003) peaks of PTO. d) The c-axis lattice parameters as a function of substrate selection. The black dashed lines in b) and d) indicate the bulk value of PTO.

lattice parameter values of their corresponding ST phases (4.77 Å) are slightly larger than the pure ST phase grown on STO, originating from larger compressive strain. More interestingly, when the growth temperature increases to 620°C, the PTO film grown on the LAO, a diffraction peak corresponding to intermediate phase (c=4.11 Å) appeared in the XRD pattern, suggesting coexistence of three phases in one sample.

To study both in-plane and out-of-plane lattice parameters, selected area electron diffraction (SAED) in transmission electron microscopy (TEM) mode was used to characterize the PTO film grown on STO (001) with substrate temperature of 600 °C, as shown in Figure 3a. Coherent epitaxial growth of PTO film with fully strain state is demonstrated. In Figure 3, the distance between PTO (002) and STO (002) peaks were measured to be 8.35 and 10.05 1/nm, respectively, corresponding c-axis lattice parameter of 4.68 Å (the slight reduction of lattice parameter compared with the XRD result, 4.71 Å, may be due to the strain relaxation in the preparation of thin TEM sample). The value is well matched with the XRD results in Figure 1. The out-of-plane to in-plane lattice parameter ratio (*c/a*) of PTO could calculated as 1.2 based on the electron diffraction analysis, the value *(c-a)/a* [%] is 20%, which is more than three times larger than the bulk form (6.5%). More comparison could be found in Table 1. The reciprocal space mapping (RSM) of the sample (103) reflection was also characterized and the result is shown in Figure S1. It shows the thin films sample is also under fully in-plane strain state.

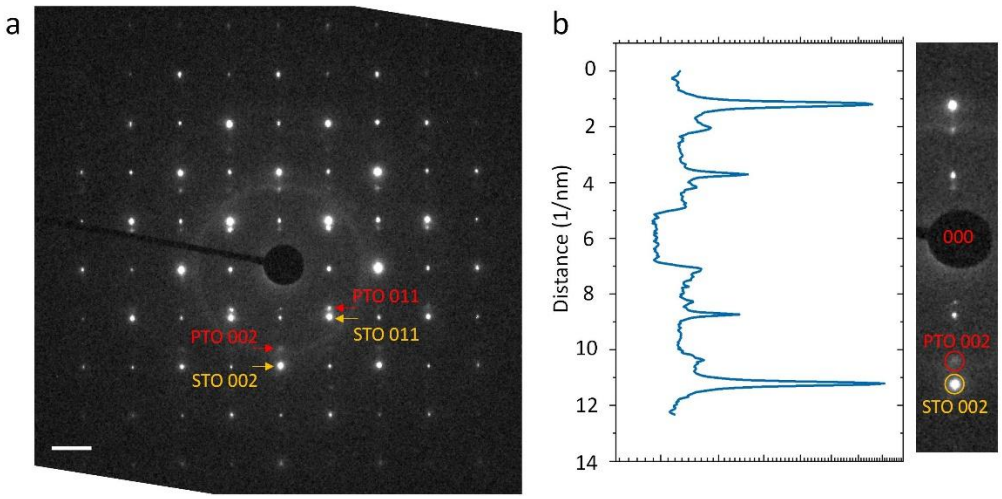

Figure 3. a) The SAED of PTO/LSMO/STO (001). b) The intensity profile of diffraction spots: PTO (002) and STO (002).

Table 1. Comparisons of lattice parameters and tetragonality [(*c*-*a*)/*a*] of perovskite ferroelectric materials.

Materials	a [Å]	c [Å]	((c-a)/a) [%]
PTO/LSMO/STO (this work)	3.9	4.71	20
(HT) PTO-LSAT (ref. 17)	3.868	4.276	10.55
PTO Bulk	3.899	4.154	6.44

To get further insights into the microstructure and ferroelectricity of the super-tetragonal PTO film, spherical aberration corrected scanning TEM (Cs corrected STEM) was conducted to investigate the atomic scale lattice structure. A low-magnification high angle annular dark field (HAADF) STEM image (Figure 4a) shows an epitaxial growth of PTO film with atomically sharp LSMO/PTO interface. More importantly, a self-assembled columnar structure could be clearly observed. Since the intensity of HAADF image is sensitive to the atomic numbers of chemical elements, the difference in contrast of the nanocolumns indicates different composition. Two types of nanocolumns can be clearly observed, denoted as type I and type II (with brighter contrast). It can be seen that the nanocolumns (type II) nucleate from the LSMO/PTO interface, and grow vertically until the film surface. The average width of the nanocolumns (type II) is ~3 nm. Figure 4b shows the high-magnification HAADF-STEM image of the nanocolumns. The interface between the two phases could be observed. To check the difference in image intensity of A-site and B-site cations , a profile of HAADF intensity was extracted in the white rectangle marked area across the nanocolumn interface along [011] direction, as shown in Figure 4c and d. As Pb has much higher atomic number Z compared with Ti, The HAADF intensity of PbO atomic column should be much higher than the TiO_2 column in $PbTiO_3$ film. It is presented that the low intensity at B-sites indicates the nanocolumn (type I) is $PbTiO_3$ phase while the high HAADF intensity of B-site suggests that a large proportion of B-sites are occupied by the Pb cations (Pb-riched) and increase the average atomic number in nanocolumn (type II). In addition, there is also a transition region of about three unit-cells thickness, possessing intermediate HAADF intensity of B-sites atomic column. It maybe originated from the overlapping between the nanocolumn phases. The analysis of the two types of nanocolumns by energy dispersive X-ray (EDX-STEM) spectrum in STEM mode was also conducted, as shown in Figure S2. The results suggest the compositions of the two regions have no evident change, both include Pb, Ti and O elements. The structure of the Pb-riched regions (nanocolumn type II) is similar to the PbO compound which has a similar tetragonal structure (a=3.899 Å, c=5.0217 Å). [22]Our chemical composition analysis suggests a high-level solution of Ti element in PbO structure. As reported in a previous study, a PbO-TiO_2 solid solution with stoichiometry of $PbTi_{0.8}O_{2.6}$ has a tetragonal structure with lattice parameters of a=0.3911 nm and c=0.4831 nm, which is close to our results. [23] The small lattice mismatch between the PbO structure phase and the manganite bottom electrode offers the possibility of its epitaxial growth along c-axis. It should also be noted that the $PbTi_{0.8}O_{2.6}$ could be converted to perovskite PTO by heating, suggesting its lower formation energy and temperature compared to perovskite phase. The

growth of self-assembled composite structure may due to the difference formation energy of these two phases: the phase with PbO structure has lower formation energy while the phase with PTO structure has higher formation energy and requires higher substrate temperature during growth. In the intermediate film growth temperature, two types of phases could be formed simultaneously with self-assembled nanostructure. The similarity in structure between PTO and PbO structure phase offers the possibility for epitaxial strain along c-axis. The PbO phase may stretch the neighboring PTO phase and elongate its c-axis lattice parameter, resulting in the formation of ST phase.

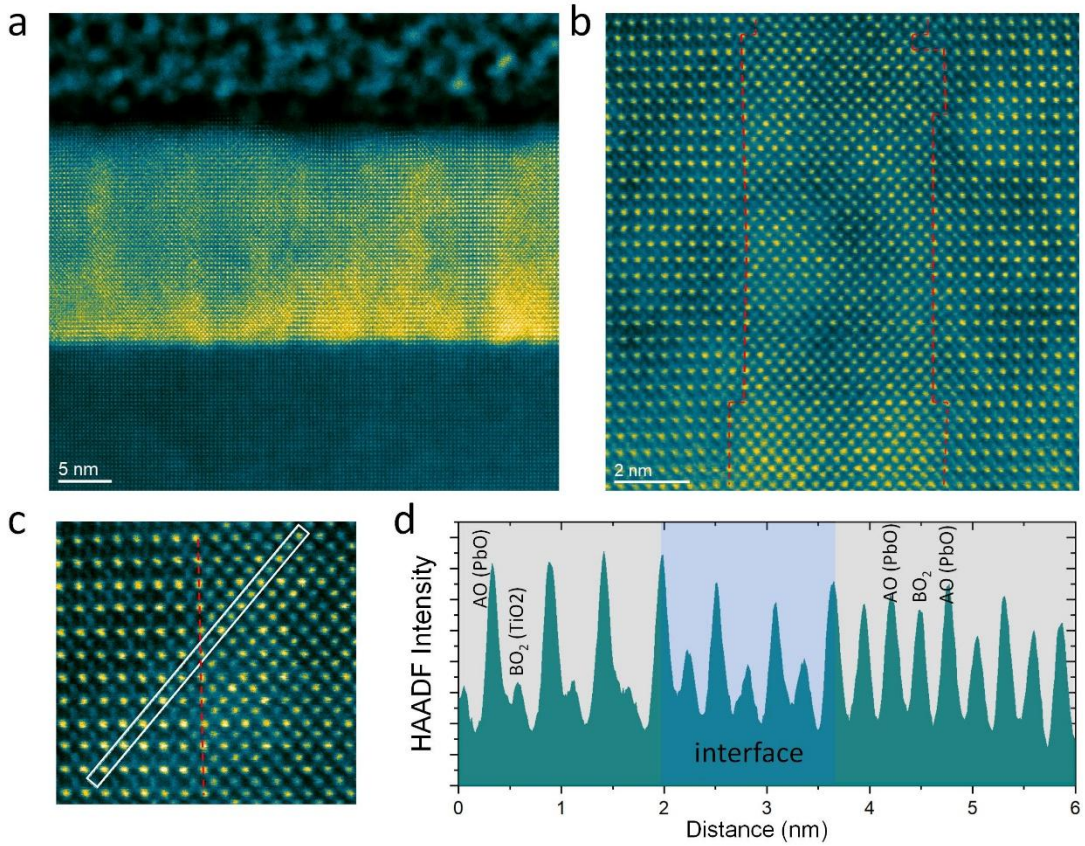

Figure 4. a) A low magnification HAADF-STEM image of PTO/LSMO/STO heterostructure. The nano-columnar structure is evident in the PTO layer. b) High resolution HAADF-STEM image of a nanocolumn. The red dashed line indicates the interface between the columnar grains. c) The enlarged HAADF-STEM image, the left side is PTO and the right side is Pb excess oxide. The red dashed line is the interface. d) The HAADF intensity profile of atomic row in c) marked by white rectangle.

Based on the measured tetragonality, a phenomenological approach was used to estimate the ferroelectricity. On the basis of the Landau−Ginzburg−Devonshire theory, ferroelectric polarization can be calculated by the equation shown below:[24]

$$P_s = \left[\frac{x_s - \frac{2s_{12}x_m}{(s_{11}+s_{12})}}{Q_{11} - \frac{2s_{12}Q_{12}}{(s_{11}+s_{12})}}\right]^{1/2} \quad (1)$$

In **Equation 1**, $x_s = (c - a_p)/a_p$; $x_m = (a - a_p)/a_p$; a and c are in-plane and out-of-plane lattice parameters; a_p, lattice parameter of cubic PTO being extrapolated to room temperature; s_{ij}, elastic compliances; Q_{ij}, electrostrictive coefficients. The values of a_p, Q_{ij}, and s_{ij} for PTO are adopted from refs 25 and 26. It could be estimated that the PTO have polarization of ~177 $\mu C/cm^2$ for the case of c/a = 1.2, which is more than two times of the PTO bulk phase. This theory was not applied to evaluate polarization before to the ferroelectrics with such high strain.

In order to study the ferroelectric properties of the PTO films, piezoelectric force microscope (PFM) analysis was used. The first sample is PTO film with pure ST phase (PTO/LSMO/STO), and the second one is PTO with coexistence of both ST and NT phases (PTO/LSMO/LSAT), the results are shown in Figure 6a and 6b, respectively. The topography in Figure 6a presents the sample has a smooth surface with roughness of 1.9 nm. The corresponding vertical PFM phase and amplitude images obtained without bias show a certain degree of change in PFM phase contrast even in the absence of an electric field, which indicates the spontaneous polarization of the film. It can be seen that the sample has *c*-oriented polarization with most area has polarization upwards and only a small portion of sample has polarization downwards. The results are consistent with the XRD and TEM analysis, which demonstrate the elongation of PTO lattices along out-of-plane direction. In contrast, Figure 6b shows different topography and PFM signal for the phase coexistence sample. The roughness of the sample surface is 3.15 nm. The PFM demonstrates a typical two-dimensional grid of 90° *c/a* domains which could be observed in conventional PTO or $PbZr_{0.2}Ti_{0.8}O_3$ (PZT) epitaxial thin films. [27,28] This PFM signal is likely from the NT phase of PTO. We conjecture that the NT phase is near surface, laying on the top of the ST phase. The formation of NT phase may originate from the epitaxial strain relaxation. The PFM analysis demonstrates that there is a good flexibility in regulating ferroelectric domain in the self-assembled nanocolumn PTO films. From an application perspective, The self-assembled nanopillar structure has well separated PTO nanocolumns, each of them could be regarded as a nonvolatile information storage unit.[29,30] The polarization direction (upwards or downwards)

represents two different memory states. The nanostructure with thickness of 3 to 5 nm could also be used in the field of ferroelectric tunnel junction devices (FTJ).[31,32] PTO nanocolumns could sever as the ferroelectric barrier layers of FTJ arrays, facilitating the development of high-density information storage devices based on ferroelectric nanocolumns.

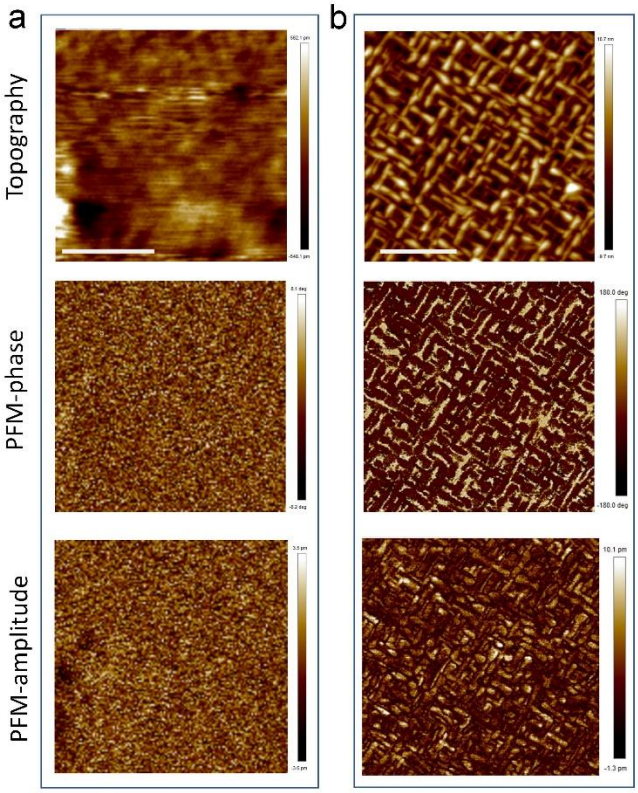

Figure 6. The topography, PFM-phase and amplitude of a) PTO/LSMO/STO and b) PTO/LSMO/LSAT. The white scale bar in the topography image is 1 μm.

3. Conclusion

In summary, we have demonstrated the growth modulation of super-tetragonal PTO films. The c-axis lattice parameter of PTO films up to 4.71 Å and *c/a* ratio of 1.2 could be achieved by tunning growth conditions, such as substrate temperature and oxygen pressure. Moreover, single lead titanate film composed of multiple tetragonalities could also be reached. The microstructure of the super-tetragonal were revealed to be self-assembled nanocolumn structure with Pb excess and matrix of $PbTiO_3$. The polarization of about ~177 μC/cm^2 is estimated for c/a = 1.2. This work provide feasibility to engineer the ferroelectric films with volatile elements with the formation of self-assembled nanostructure without the limitation of commercially discrete single crystal substrates. We also emphasize that the strategy could be widely applicable to growth of other electronic materials to extend the lattice control with emergent functionalities.

4. Experimental Section

Film Growth: The epitaxial $PbTiO_3$ (PTO) films were grown by pulsed laser deposition (PLD). The samples of $La_{0.3}Sr_{0.7}MnO_3$ (20 nm)/$PbTiO_3$(18/36/54 nm) were grown on $SrTiO_3$ (001) [STO (001)] substrates using pulsed laser deposition (PLD). The bottom layer of LSMO was deposited first and acted as the bottom electrode for the LSMO/PTO stack. The films of LSMO and PTO were epitaxially grown by PLD using a KrF laser with a repetition rate of 3 Hz and a fluence around 1.5 J cm^{-2}. During the deposition, the temperature was kept at 780 °C for LSMO and (T_p=540/570/600/630/700℃) for PTO. After deposition, the oxygen pressure was raised to 5000Pa, kept there for 10 min, and then the films were cooled down in oxygen (5000 Pa) to room temperature with 5 °C min^{-1}.

Characterization: The X-ray diffraction (XRD) measurements were performed on a D8 Advance diffractometer (Bruker Corporation, Germany), operating at 40 kV and 40 mA with Cu Ka radiation (λ=1.5406 Å). The scanning rate for phase identification was fixed at 5° min^{-1} with a 2θ range from 10° to 90°, and the data for analyzing were collected in a step-scanning mode with a step size of 0.02°.

The cross-sectional TEM samples were prepared by focused ion beam milling method, followed by argon ion milling in Leica EM RES102 Multifunctional Ion Milling System at 0.5 kV to reduce the damaged layer.. Selected-area electron diffraction (SAED) and high angle annular dark field (HAADF) imaging were performed on a spherical-aberration corrected JEOL ARM 200F scanning transmission electron microscope, operated at 200 kV. For HAADF imaging a probe size of 0.1 nm was used with a semi-convergence angle of α = 22 mrad. The angular detector used for HAADF imaging had an angular area for capturing the electrons with scattering angles in a range of 90-176 mrad.

The PFM measurement was conducted on Bruker Dimension Icon AFM. Conductive DDESP (spring constant: 80 N/m, frequency: 450 KHz) probe was used and AC modulation of 3000 mV at 15 kHz was applied to the probe. Piezeo-response from the material was monitored by a photodiode using the lock-in amplifier technique. Sample was scanned at 0.5 Hz rate.

Supporting Information

Supporting information is available from the Wiley Online Library or from the author.

Acknowledgements

This work was financially supported by the National Key Research and Development Program of China (Grant No. 2019YFB2005801, 2016YFA0300804), the National Natural Science Foundation of China (Grants No. 51731003, No. 51971023, No. 51927802, No. 11974023, No. 52061135205) and the Fundamental Research Funds for the Central Universities (FRF-TP-19-012B1).

Conflict of Interest

The authors declare no conflict of interest.

Data Availability Statement

Research data are not shared.

Keywords: ferroelectrics, lead titanate, elastic coupling, self-assembled nanostructure

Received: ((will be filled in by the editorial staff))
Revised: ((will be filled in by the editorial staff))
Published online: ((will be filled in by the editorial staff))

References

[1] T. Ma, J. Gou, S. Hu, X. Liu, C. Wu, S. Ren, H. Zhao, A. Xiao, C. Jiang, X. Ren, M. Yan, *Nat. Commun.* **2017**, *8*, 13937.

[2] D. Meng, H. Guo, Z. Cui, C. Ma, J. Zhao, J. Lu, H. Xu, Z. Wang, X. Hu, Z. Fu, R. Peng, J. Guo, X. Zhai, G. J. Brown, R. Knize, Y. Lu, *Proc. Natl. Acad. Sci. USA* **2018**, *115*, 2873-2877.

[3] A. R. Damodaran, E. Breckenfeld, Z. Chen, S. Lee, L. W. Martin, *Adv. Mater.* **2014**, *26*, 6341-6347.

[4] E. Y. Tsymbal, H. Kohlstedt, *Science* **2006**, *313*, 181-183.

[5] Scott, J. F., Applications of Modern Ferroelectrics. *Science* **2007**, 315, 954-959.

[6] H. Béa, B. Dupé, S. Fusil, R. Mattana, E. Jacquet, B. Warot-Fonrose, F. Wilhelm, A. Rogalev, S. Petit, V. Cros, A. Anane, F. Petroff, K. Bouzehouane, G. Geneste, B. Dkhil, S. Lisenkov, I. Ponomareva, L. Bellaiche, M. Bibes, A. Barthélémy, *Phys. Rev. Lett.* **2009**, *102*, 217603.

[7] R. J. Zeches, M. D. Rossell, J. X. Zhang, A. J. Hatt, Q. He, C-H. Yang, A. Kumar, C. H. Wang, A. Melville, C. Adamo, G. Sheng, Y-H. Chu, J. F. Ihlefeld, R. Erni, C. Ederer, V. Gopalan, L. Q. Chen, D. G. Schlom, N. A. Spaldin, L. W. Martin, R. Ramesh, *Science* **2009**, *326*, 977-980.

[8] J. X. Zhang, Q. He, M. Trassin, W. Luo, D. Yi, M. D. Rossell, P. Yu, L. You, C. H. Wang, C. Y. Kuo, J. T. Heron, Z. Hu, R. J. Zeches, H. J. Lin, A. Tanaka, C. T. Chen, L. H. Tjeng, Y.-H. Chu, R. Ramesh, *Phys. Rev. Lett.* **2011**, *107*, 147602.

[9] A. B. Alexei, A. Masaki, S. Takashi, S. Yuichi, T. Mikio, *Chem. Mater.* **2005**, *17*, 269-273.

[10] C. Ederer, N. A. Spaldin, *Phys. Rev. Lett.* **2005**, *95*, 257601.

[11] Z. Chen, Z. Luo, C. Huang, Y. Qi, P. Yang, L. You, C. Hu, T. Wu, J. Wang, C. Gao, T. Sritharan, L. Chen, *Adv. Funct. Mater.* **2011**, *21*, 133-138.

[12] D. G. Schlom, C. J. Fennie, *Nat. Mater.* **2015**, *14*, 969-970.

[13] Y. Tang, Y. Zhu, X. Ma, Z. Hong, Y. Wang, W. Wang, Y. Xu, Y. Liu, B. Wu, L. Chen, C. Huang, L. Chen, Z. Chen, H. Wu, *Adv. Funct. Mater.* **2019**, *29*, 1901687.

[14] A. A. Belik, I. Satoshi, K. Katsuaki, I. Naoki, S.-I. Shamoto, N. Seiji, A. Masaki, S. Yuichi, T. Mikio, I. Fujio, F. Izumi, T.-M. Eiji, *Chem. Mater.* **2006**, *18*, 798-803.

[15] J. H. Lee, L. Fang, E. Vlahos, X. Ke, Y. W. Jung, L. F. Kourkoutis, J.-W. Kim, P. J. Ryan, T. Heeg, M. Roeckerath, V. Goian, M. Bernhagen, R. Uecker, P. C. Hammel, K. M. Rabe, S. Kamba, J. Schubert, J. W. Freeland, D. A. Muller, C. J. Fennie, P. Schiffer, V. Gopalan, E. Johnston-Halperin, D. G. Schlom, *Nature* **2010**, *466*, 954-958.

[16] D. G. Schlom, L.-Q. Chen, C.-B. Eom, K. M. Rabe, S. K. Streiffer, J.-M. Triscone, *Annu. Rev. Mater. Res.* **2007**, *37*, 589-626.

[17] C. Huang, Z. Liao, M. Li, C. Guan, F. Jin, M. Ye, X. Zeng, T. Zhang, Z. Chen, Y. Qi, P. Gao, L. Chen, *Adv. Sci.* **2021**, *8*, 2003582.

[18] Y. Wang, J. M. Hu, Y. H. Lin, C.-W. Nan, *NPG Asia Mater*. **2010**, *2*, 61-68.

[19] J. L. Lin, R. He, Z. Lu, Y. Lu, Z. Wang, Z. Zhong, X. Zhao, R.-W. Li, Z. D. Zhang, Z. J. Wang, *Acta Mater.* **2020**, *199*, 9-18.

[20] L. Zhang, J. Chen, L. Fan, O. Dieguez, J. Cao, Z. Pan, Y. Wang, J. Wang, M. Kim, S. Deng, J. Wang, H. Wang, J. Deng, R. Yu, J. F. Scott, X. Xing, *Science* **2018**, *361*, 494-497.

[21] S. A. Mabud, A. M. Glazer, *J. Appl. Cryst.* **1979**, *12*, 49-53.

[22] H. E. Swanson, R. K. Fuyat, *Natl. Bur. Stand.* **1953**, *539*, 30-33.

[23] H. Cheng, J. Ma, Z. Zhao, *Chem. Mater.* **1994**, *7*, 1033-1040.

[24] C. L. Jia, S. B. Mi, K. Urban, I. Vrejoiu, M. Alexe, D. Hesse, *Phys. Rev. Lett.* **2009**, *102*, 117601.

[25] Y. L. Tang, Y. L. Zhu, X. L. Ma, A. Y. Borisevich, A. N. Morozovska, E. A. Eliseev, W. Y. Wang, Y. J. Wang, Y. B. Xu, Z. D. Zhang, S. J. Pennycook, *Science* **2015**, *348*, 547-551.

[26] G. Shirane, S. Hoshino, *J. Phys. Soc. Jpn.* **1951**, *6*, 265-270.

[27] C. S. Ganpule, V. Nagarajan, H. Li, A.S. Ogale, D.E. Steinhauer, S. Aggarwal, E. Williams, R. Ramesh, *Appl. Phys. Lett.* **2000**, *10*, 292.

[28] X. Lu, Z. Chen, Y. Cao, Y. Tang, R. Xu, S. Saremi, Z. Zhang, L. You, Q. Dong, S. Das, H. Zhang, L. Zheng H. Wu, W. Lv, G. Xie, X. Liu, J. Li, L. Chen, L. Chen, W. Cao, L.W. Martin, *Nature Commun*. **2019,** *10*, 3951.

[29] A. I. Khan, A. Keshavarzi, S. Datta, *Nat. Electron.* **2020**, *3*, 588-597.

[30] J. F. Scott, C. A. P. Araujo, *Science* **1989**, *246*, 4936.

[31] V. Garcia, M. Bibes, *Nat. Commun.* **2014**, *5*, 4289.

[32] V. Garcia, S. Fusil, K. Bouzehouane, S. Enouz-Vedrennez, N. D. Mathur, A. Barthélémy, M. Bibes, *Nature* **2009**, *460*, 81-84.

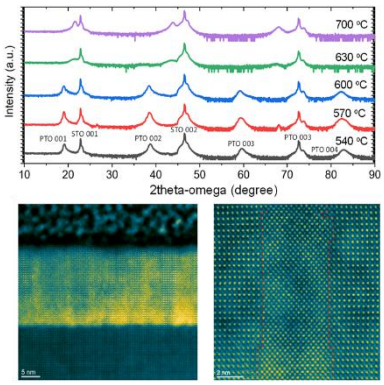

Short summary: Ferroelectric epitaxial thin films composed of self-assembled arrays of $Pb_xTi_yO_{x+2y}$ nanocolumns embedded in a $PbTiO_3$ matrix could be fabricated by laser ablation. The c-axis lattice parameter of the whole nanostructure up to 4.7 Å and the out-of-plane to in-plane lattice parameter ratio of 1.2 could be achieved. This work provides a general approach to regulation of lattice states and functionalities beyond their present levels via elastic coupling between the self-assembled nanostructures in three dimensions.